International Journal of
Science and Engineering Investigations vol. 6, issue 61, February 2017
ISSN: 2251-8843

Design and Performance Investigation of Graphene-Based Modulators for 1550 and 1310 nm Optical Communication Wavelengths

Taif Aied Faisal[1], Raad Sami Fyath[2]
[1]Laser and Optoelectronics Engineering Department, Al-Nahrain University, Baghdad, 00964, Iraq
[2]Computer Engineering Department, Al-Nahrain University, Baghdad, 00964, Iraq
([1]taif.alawsi@outlook.com, [2]rsfyath@yahoo.com)

Abstract- This paper addresses the design and performance investigation of grapheme-based optical modulators (GBOMs) for 1550 and 1310 nm optical communication wavelengths. The design stands heavily on two commercial software packages, namely COMSOL Multiphysics and LUMERICAL. The graphene optoelectronic properties, such as surface conductivity, relative permittivity, and refractive index, are first calculated theoretically as a function of operating wavelength and applied voltage. These calculations are useful to model the graphene as a new element in the software package element library. Accordingly, four GBOMs configurations are designed, two waveguide modulators (WGMs) and two Mach-Zehnder modulators (MZMs). Each modulator is based on either square or rectangular cross section silicon waveguide covered with a graphene layer. The calculations and simulation results reveal that the modulator bandwidth is enhanced by 50 % at 1550 nm and 35 % at 1310 nm when the square waveguide is replaced by a rectangular one. Further, both WGM and MZM modulators have almost the same bandwidth. At 1550 nm wavelength, the waveguide modulator offers 324.4 and 162.2 GHz bandwidth for 100- and 200 µm-waveguide lengths, respectively.

Keywords- *Graphene Optical Modulator, Mach-Zehnder Modulator, Waveguide Modulator, COMSOL Multiphsics, Graphene Surface Conductivity.*

I. INTRODUCTION

Graphene is a two-dimensional (2D) allotrope of carbon that has a honeycomb-like structure. It has unique electrical, optical, mechanical, and chemical properties that makes it suitable for many applications including photonics, electronics and optoelectronics devices and components [1-10]. Graphene can enhance the optical modulator by implementing the material inside the modulator leading to high modulation depth, high seed operation, low insertion loss, low operating voltage, and compact footprint [11-15].

The concept of graphene-based optical modulator (GBOM) took a great interest in the research from the late 2000's. The researchers around the world designed much novel architecture each has its own characteristics and limitations, yet no group reached to the optimum requirements due to high demands of electronics, photonics, plasmonics and communication fields. The electrical demands of the modulator needed to be much less and the data transfer rates needed to be as much as it can be. In theory, many groups may have reached a high advance, but practically speaking many problems can occur due to the integration of the electronics-photonics system, which must be a small footprint and less noise.

There are many theoretical studies reported in the literature related to GBOMs. Zhu et al. [10] demonstrated theoretically an advanced optical modulator based on graphene with voltage controllable reflections. The optical signal transmitted through the graphene was modulated by dynamically varying the graphene's effective permittivity via the voltage biasing of the Fermi level. They showed that their modulation technique is capable of providing a relative reflectance change of 361%. Gao et al. [11] demonstrated theoretically a high-contrast electro-optic modulation in a graphene integrated photonic crystal nanocavity, providing a modulation depth of more than 10 dB at telecom wavelengths. Zhou et al. [12] studied numerically the graphene enhanced fiber-optic phase modulator with a novel architecture that proved a wide linear dynamic range with an arm length of 127 µm. Ye et al. [13] studied theoretically and numerically dual graphene-on-graphene electro-absorption optical modulator with four layers of graphene embedded in a silicon-on-insulator (SOI) waveguide. They showed that their proposed structure is able to achieve 34 dB extinction ratio (ER) and 100 GHz of modulation bandwidth with an energy consumption of 17.6 fJ/bit. Du et al. [14] analyzed theoretically the graphene-based ring modulator. They found a very high tunability of (1.08 nm/V) that can be achieved due to the enlarged effective refractive index of the waveguide, a large ER of 22.13 dB and operation bandwidth up to 149 GHz. The modulator has a wide resonance wavelength shift with a 27 K temperature tolerance. Midrio et al. [18] reported an electro-refractive modulator based on single- and double-layer graphene on top of silicon waveguides. They showed that the proposed devices might theoretically outperform existing modulators both in terms of $V_\pi L_\pi$ and of insertion losses. The overall figures of merit of the proposed devices are as low as 8.5 and 2dB•V for the single-

and double-layer cases, respectively. Pan et al. [19] demonstrated numerically a compact high-speed electro-optic modulator based on a silicon photonic crystal nanobeam cavity with gated graphene on top. They showed that their proposed modulator could provide a large free spectral range up to 125.6 nm, a high modulation depth of 12.5 dB, and a high modulation speed of 133 GHz.

Few experimental results related to GBOMs have been reported in the literature. For example, Hu et al.[20] studied practically the graphene electro-absorption modulator with 10 Gb/s of modulation speed. A new design was introduced that can work over a wide range of wavelengths and temperatures. The proposed modulator was used for chip-level optical interconnect. Mohsin et al. [21] demonstrated experimentally a graphene based electro-absorption modulator with very low insertion loss. The device was realized on a silicon-on-insulator (SOI) waveguide operating at 1550 nm wavelength. The modulator shows a modulation depth of 16 dB and an insertion loss of 3.3 dB. Mohsin et al. [22] designed an electro-refractive phase modulator operating in the wavelength range of 1530-1570 nm. The refractive index was realized experimentally using graphene as active material. Phare et al. [23] demonstrated an ultrafast graphene modulator by leveraging critical coupling effects on a silicon nitride ring resonator. This modulator achieves a figure of merit of 3.75 GHz V^{-1}, compared to 0.16 GHz V^{-1} in low insertion loss graphene-on-silicon structures and 0.27 GHz V^{-1} in double-layer graphene electro-absorption devices.

The aim of this paper is to design and investigate the performance of graphene-based optical modulators for 1550 and 1310 nm optical communication wavelengths. The design uses theoretical modeling of graphene optoelectronic properties coupled to commercial software packages.

II. GRAPHENE OPTOELECTRONIC PROPERTIES

In this section, the surface conductivity σ_g, the relative permittivity ε_g, and the refractive index n_g, are calculated for graphene as a function of the applied voltage V_g. The results are provided for 1550 nm and 1310 nm wavelengths using the following parameter values

Voltage offset (V_0) = 0.8 V.

Fermi velocity (v_f) = 10^6 m.s^{-1}.

Scattering rate (Γ) = 10^{12} s^{-1}.

Graphene layer thickness (d) = 0.34 nm.

Graphene surface conductivity (σ_g) has two types of conductivity according to the transition that occurred in the graphene material, namely intraband (σ_a) and interband (σ_e) [24]

$$\sigma_g(\omega) = \sigma_a(\omega) + \sigma_e(\omega) \tag{1}$$

The conductivity of graphene depends on the frequency (ω) [25-38]

$$\sigma_a(\omega) = \frac{e^2}{j\pi\hbar^2(\omega + j2\Gamma)} \int_0^{+\infty} E\left(\frac{df_e(E)}{dE} - \frac{df_e(-E)}{dE}\right)dE \tag{2a}$$

$$\sigma_e(\omega) = j\frac{e^2(\omega + j2\Gamma)}{\pi\hbar^2} \int_0^{+\infty} \frac{f_e(-E) - f_e(E)}{(\omega + j2\Gamma)^2 - 4(E/\hbar)^2} dE \tag{2b}$$

where f_e (E) is the Fermi-Dirac distribution function and its expressed as

$$f_e(E) = \frac{1}{e^{(E-\mu_C)/K_BT} + 1} \tag{3}$$

Here, E is the energy, μ_C is the chemical potential, K_B is the Boltzmann's constant, T is the temperature, $\hbar$ is the modified Planck's constant, ω is the frequency, and Γ is the scattering rate.

The graphene surface conductivity can be written separately as four equations representing the derived expressions of the real and imaginary parts of the graphene intraband and interband conductivities, respectively.

$$\sigma_{ar} = \mathrm{Y}_{ar}\mu_C + 2\mathrm{Y}_{ar}K_BT\left(In\left(e^{-\frac{\mu_C}{K_BT}} + 1\right)\right) \tag{4a}$$

$$\sigma_{ai} = \mathrm{Y}_{ai}\mu_C + 2\mathrm{Y}_{ai}K_BT\left(In\left(e^{-\frac{\mu_C}{K_BT}} + 1\right)\right) \tag{4b}$$

$$\sigma_{er} = \frac{\sigma_0}{\pi}\tan^{-1}\left(\frac{\vartheta_1}{\vartheta_2}\right) \tag{4c}$$

$$\sigma_{er} = -\frac{\sigma_0}{2\pi}\ln\left(\frac{\vartheta_1^2 + \vartheta_2^2}{\vartheta_3^2}\right) \tag{4d}$$

where σ_{ar} is the real part of the intraband conductivity, σ_{ai} is the imaginary part of the intraband conductivity, σ_{er} is the real part of the interband conductivity, σ_{ei} is the imaginary part of the interband conductivity. In addition, the other parameters of the equations are described in following equations

$$\sigma_0 = \frac{e^2}{4\hbar} = 60.8\mu S \tag{5}$$

where σ_0 is the universal optical conductivity of the graphene, it is used to provide the relative conductivity of the graphene material by dividing the required surface conductivity on the universal optical conductivity as will be shown in the results later.

$$\mathrm{Y}_{ar} = \frac{4\sigma_0\Gamma}{\omega^2 - 4\Gamma^2} \tag{6a}$$

$$\mathrm{Y}_{ai} = \frac{\sigma_0\omega}{\omega^2 - 4\Gamma^2} \tag{6b}$$

where γ_{ar} and γ_{ai} are conductivity rate numerical parameters used for the intraband conductivity calculations of the real and imaginary parts, respectively.

$$\vartheta_1 = 4\mu_C^2 - \hbar^2\omega^2 - (2\hbar\Gamma)^2 \tag{7a}$$

$$\vartheta_2 = 4\hbar\Gamma\mu_C - 2\hbar^2\Gamma\omega - (2\hbar\Gamma)^2 \tag{7b}$$

$$\vartheta_3 = (2\mu_C + \hbar\omega)^2 + (2\hbar\Gamma)^2 \quad (7c)$$

where

σ_0 = Universal optical conductivity

The permittivity of graphene depends on the graphene surface conductivity, the frequency of operating, and the thickness of the graphene material. For single-layer graphene, the thickness is considered as 0.34 nm and the equation that predicts the permittivity behaviour with the chemical potential of graphene is

$$\varepsilon_g(\omega) = 1 + \frac{j\sigma_g(\omega)}{\omega d \varepsilon_0} \quad (8)$$

Since the permittivity is a complex, it can be written as shown in equation 9a.

$$\varepsilon_g(\omega) = \varepsilon_{gr}(\omega) + j\varepsilon_{gi}(\omega) \quad (9a)$$

where

$$\varepsilon_{gr}(\omega) = 1 - \frac{\sigma_{gi}(\omega)}{\omega d \varepsilon_0} \quad (9b)$$

$$\varepsilon_{gi}(\omega) = \frac{\sigma_{gr}(\omega)}{\omega d \varepsilon_0} \quad (9c)$$

where

$\varepsilon_g(\omega)$ = Graphene permittivity

$\varepsilon_{gr}(\omega)$ and $\varepsilon_{gi}(\omega)$ = Real and imaginary parts of graphene permittivity, respectively

$\sigma_{gr}(\omega)$ and $\sigma_{gi}(\omega)$ = Real and imaginary parts of graphene surface conductivity, respectively

ε_0 = Dielectric constant of free space

d = Thickness of graphene material

$\sigma_g(\omega)$ = Graphene surface conductivity

ω = Radian frequency.

The refractive index of graphene is the root square of the graphene conductivity and it can be represented by real and imaginary parts as n_{gr} and n_{gi}, respectively

$$n_g(\omega) = \sqrt{\varepsilon_g(\omega)} \quad (10a)$$

$$n_g(\omega) = n_{gr}(\omega) + jn_{gi}(\omega) \quad (10b)$$

Figures 1a and 1b show the relation between chemical potential and applied voltage for different values of energy hopping parameter and layer thickness, respectively. The minimum value of μ_C lies at the Dirac point with 0 eV at the energy hopping parameter (γ_{AB}) value of -3.3 eV.

The results show that the chemical potential increases with applied voltage, if the applied voltage is more than the absolute value of the Dirac voltage $V_0 = V_{Dirac}$ which is taken as 0.8 V. Figure 1b shows the variation of chemical potential with applied voltage for different layer thicknesses with minimum value of 0 eV at the Dirac point and at 70 nm layer thickness.

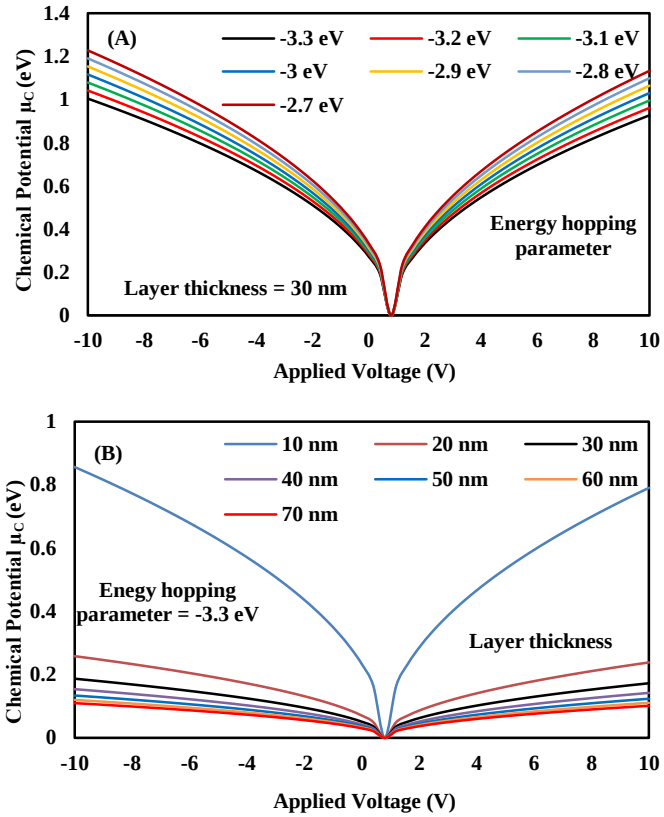

Figure 1. Graphene chemical potential as a function of applied voltage for different values of (a) energy hopping parameter (b) layer thickness.

A. Graphene Surface Conductivity

Figure 2 shows the surface conductivity of the graphene as a function of applied voltage with the differentiation between intraband (real and imaginary parts) and the interband (real and imaginary parts).

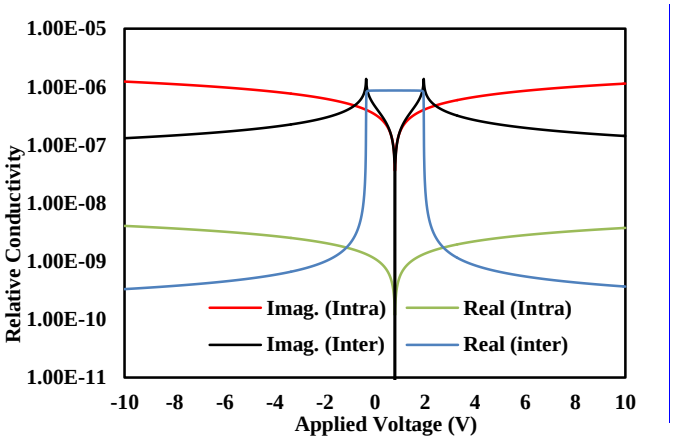

Figure 2. Graphene surface conductivity as a function of applied voltage at 1550 nm operating wavelength.

The results are based on equations 4a-d and calculated at 1550 nm wavelength. At the zero potential, the real part of the intraband conductivity takes the minimum value of conductivity, while the real part of the interband conductivity takes the maximum value of conductivity. The in-between values are the imaginary parts of the intraband and interband, respectively. The intraband conductivity has a fixed separation between its real and imaginary part, while the interband conductivity intersects at the absolute value of -0.303 eV as shown in the Fig. 2. The figure also shows a symmetric behaviour upon the offset voltage. The relative conductivity is for scaling of parameters by dividing the conductivities on the universal optical conductivity (σ_0) of graphene.

The dependence of the real and imaginary parts of the total graphene surface conductivity on the applied voltage is given in Fig. 3 for λ=1550 nm.

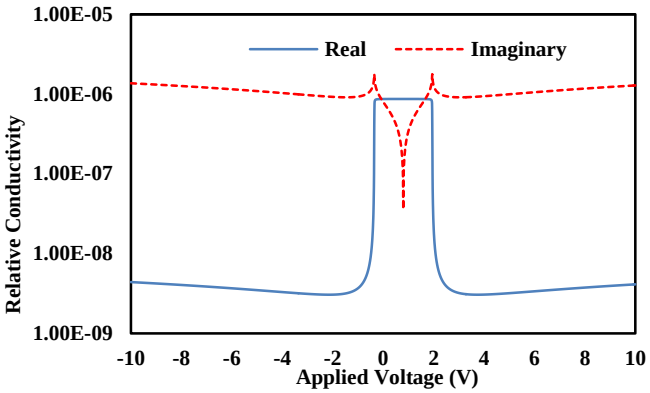

Figure 3. Real and imaginary parts of total graphene conductivity as a function of applied voltage at 1550 nm wavelength.

Fig. 3 shows the same symmetry around the offset voltage of graphene and gives another picture of the representation of graphene surface conductivity. In addition, it proves the derived equations of our mathematical modeling of the surface conductivity. The real part of the total surface conductivity starts from 4.36 X 10^{-9} then it decays slowly to reach 3.32 X 10^{-9} at the applied voltage of -1 V. After that it rises rapidly to reach its maximum value 7.91 X 10^{-7} when the applied voltage reaches 0.31 V and remain constant when the voltage reaches 1.68. Then it decays rapidly to reach 3.64 X 10^{-9} when the applied voltage reaches 2.57 V. After that it rises slowly to reach 4.1 X 10^{-9} when the applied voltage reaches 10 V. On the other hand, the imaginary part of the total surface conductivity starts from 1.36 X 10^{-6} at -10 V then it decays slowly to reach 9.23 X 10^{-7} at -1 V. Then it reaches the peak value of 1.77 X 10^{-6} at -0.35 V. Then it reaches its minimum value of 3.6 X 10^{-8} at 0.8 V – the offset voltage value -. Then it repeats the symmetric behaviour on the offset voltage value.

At the operating wavelength λ=1550 nm, the absolute value of graphene's chemical potential $|\mu_C|$= 0.39 eV at which the real part and the imaginary part of the interband conductivity intersects as shown in Fig. 2. While at the operating wavelength λ=1310 nm, the absolute value of graphene's chemical potential $|\mu_C|$= 0.4625 eV at which the real part and the imaginary part of the interband conductivity intersects as shown in Fig. 4. These intersection points are favorable in the operating wavelength of choice. Another interesting point is the intersection point of the real parts of intraband and interband conductivity. For λ=1550 nm this point occurs at the $|\mu_C|$= 0.5205 eV and for λ=1310 nm this point occurs at the $|\mu_C|$= 0.616 eV.

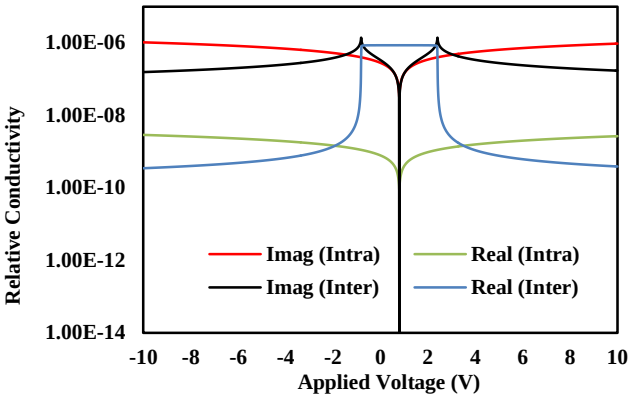

Figure 4. Graphene conductivity as a function of applied voltage at the 1310 nm operating wavelength.

At the operating wavelength λ=1310 nm, the real part of the total surface conductivity starts from 3.23 X 10^{-9} at -10 V. Then it decays slowly to reach 2.75 X 10^{-9} at the applied voltage of -2.09 V. After that it rises rapidly to reach its maximum value 8.67 X 10^{-7} when the applied voltage reaches 0.77 V and remains constant when the voltage reaches 2.39 V. Then it decays rapidly to reach 2.72 X 10^{-9} this is when the applied voltage reaches 3.48 V. After that it rises slowly to reach 3.06 X 10^{-9} when the applied voltage reaches 10 V. On the other hand, the imaginary part of the total surface conductivity starts from 1.19 X 10^{-6} at -10 V then it decays slowly to reach 9.22 X 10^{-7} at -1.8 V. Then it reaches the peak value of 1.81 X 10^{-6} at -0.81 V. Then it reaches its minimum value of 3.04 X 10^{-8} at 0.8 V – the offset voltage value -. Then it repeats the symmetric behaviour on the offset voltage value as shown in Fig. 5.

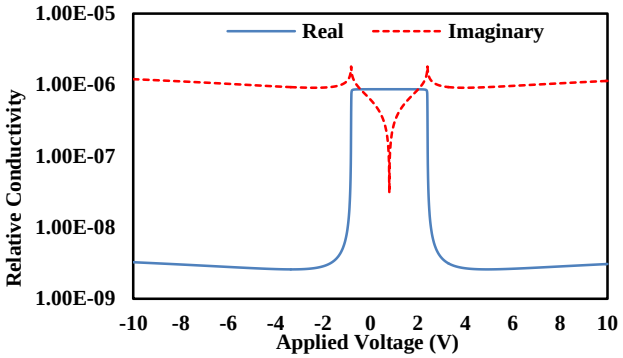

Figure 5. Real and imaginary parts of total graphene conductivity as a function of applied voltage at 1310 nm wavelength.

B. *Graphene Permittivity*

Fig. 6a and 6b show the relation between the permittivity of graphene and the applied voltage for the operating wavelength of 1550 nm and 1310 nm, respectively. Comparison between these two figures indicates that the real part of the permittivity takes a larger value with an increase of operating wavelength (7.2 for 1550 nm and 6.587 for 1310 nm) and also shifts its peak voltage from (0.49 V to 0.508 V which occur at 1550 nm to 1310 nm). These wavelengths represent the operating wavelengths of the optical communication systems.

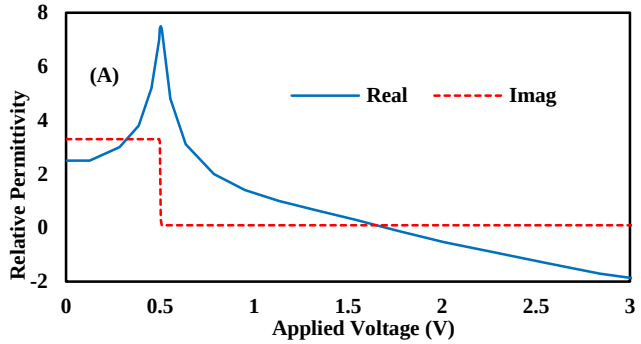

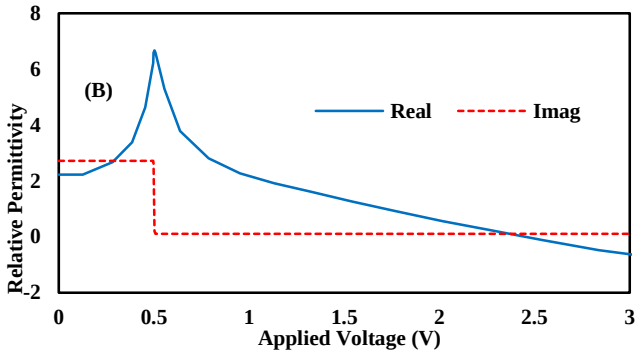

Figure 6. Graphene permittivity as a function of applied voltage at (a) 1550 nm (b) 1310 nm.

C. *Graphene Refractive Index*

Fig. 7a and 7b show the relation between the refractive index of graphene and the applied voltage for 1550 nm and 1310 nm, respectively.

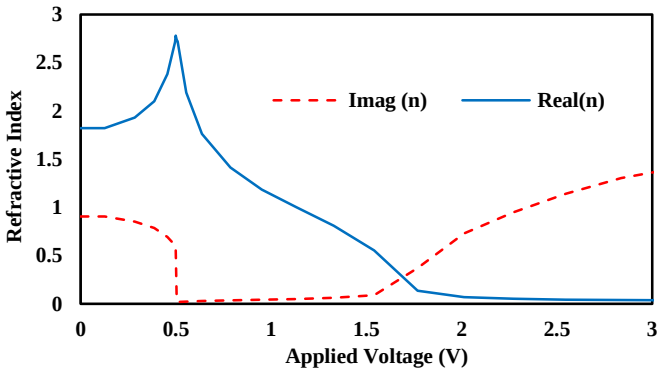

Figure 7. a) Graphene refractive index as a function of applied voltage at the operating wavelength 1550 nm.

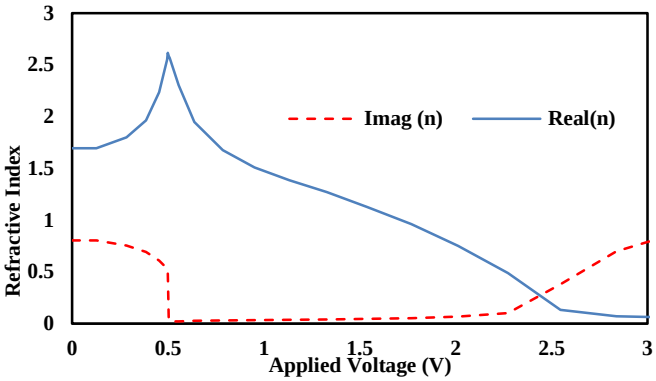

Figure 7. b) Graphene refractive index as a function of applied voltage at the operating wavelength 1310 nm.

Comparison between Fig. 7a and 7b shows that the real part of the refractive index takes a larger value with increasing the operating wavelength (2.71 for 1550 nm and 2.58 for 1310 nm) and also shifts its peak voltage from (0.49 V to 0.508 V which occur at 1550 nm to 1310 nm).

TABLE I. DEPENDENCE OF GRAPHENE RELATIVE PERMITTIVITY AND REFRACTIVE INDEX ON THE APPLIED VOLTAGE.

Applied Voltages (V)	Relative Permittivity ($\varepsilon_g = \varepsilon_{gr} + j\varepsilon_{gi}$)		Refractive Index ($n_g = n_{gr} + jn_{gi}$)	
	λ= 1550 nm	*λ= 1310 nm*	*λ= 1550 nm*	*λ= 1310 nm*
-40	1.888587 + 0.002446i	1.626435 + 0.0014908i	1.37425+ 0.00089i	1.275317 + 0.0005845i
-30	1.763672 + 0.002141i	1.535872 + 0.001309i	1.32803 + 0.000809i	1.239303 + 0.0005281i
-20	1.61445 + 0.00178i	1.426996 + 0.001099i	1.27061 + 0.000703i	1.1945697 + 0.00046024i
-10	1.41484 + 0.00134i	1.278905 + 0.0008474i	1.18947 + 0.00056i	1.130887 + 0.00037469i
0	0.96304 + 0.28034i	0.985959+ 0.2371i	0.99148 + 0.141376i	1.0000073 + 0.1185528i
10	1.37261 + 0.00126i	1.2468623 + 0.000802i	1.17158 + 0.00053i	1.1166299 + 0.0003593i
20	1.58691 + 0.00172i	1.4067686 + 0.001062i	1.25972 + 0.00068i	1.1860728 + 0.00044782i
30	1.74185 + 0.00208i	1.5200108 + 0.001277i	1.319794 + 0.000791i	1.2328873 + 0.0005182i
40	1.86997 + 0.00241i	1.61296265 + 0.001463i	1.367469 + 0.0008778i	1.2700247 + 0.0005761i

Table 1 lists the values of the refractive index (n_g) and the relative permittivity (ε_g) as a function of applied voltage ranging from -40 to 40 V in 10 volts steps for the operating wavelengths of λ= 1550 nm and 1310 nm. These values will be used to model the graphene as a library element in the used software packages.

III. Design of Graphene-Based Optical Modulators

This section presents the design GBOMs for 1550 and 1310 nm wavelengths. The design uses waveguide modulator (WGM) and Mach-Zehnder modulator (MZM) configurations and stands heavily on commercial software packages, namely COMSOL and LUMERICAL.

The modulators are designed in three-dimensional (3D) environment. Four modulator structures are designed with silicon waveguides having square or rectangular cross section as shown in Fig. 8 a-d.

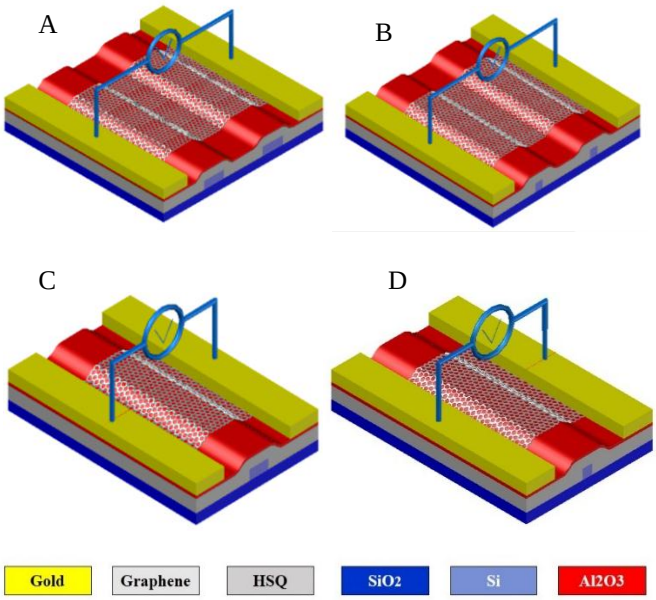

Figure 8. 3D GBOM designed with a. two rectangular waveguides b. two square waveguides c. one rectangular waveguide d. one square waveguide.

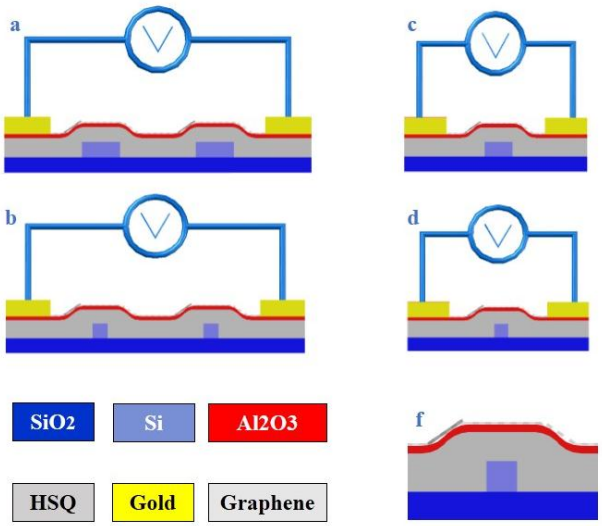

Figure 9. 2D representation of GBOM designed with a. two rectangular waveguides b. two square waveguides c. one rectangular waveguide d. one square waveguide f- Magnified image for graphene illustration.

The design takes into consideration the shape of the waveguide (to be square and rectangle), the number of waveguides (to be one or two), the electrode contact material (to be gold or nickel), the buffer layer material (to be hydrogen silsesquioxane (HSQ) or hafnium dioxide - yttrium oxide (HfO2-Y2O3)). Interchangeably, the work focuses on these parameters and their effect upon the modulator characteristics. Performance comparison among those modulators is performed to achieve the optimum desired features for the required operation. Fig. 4 shows the modulators in a comparative two-dimensional (2D) representation.

The COMSOL design of the rectangular waveguide modulator is illustrated in the following steps.

i. Use SiO_2 as the base layer and add Si waveguide on top of it, (Fig. 10a).

ii. Add HSQ as a buffer layer material (Fig. 10b).

iii. Add graphene material on top of the HSQ layer (Fig. 10c).

iv. Use Al_2O_3 material on top of the structure (Fig. 10d).

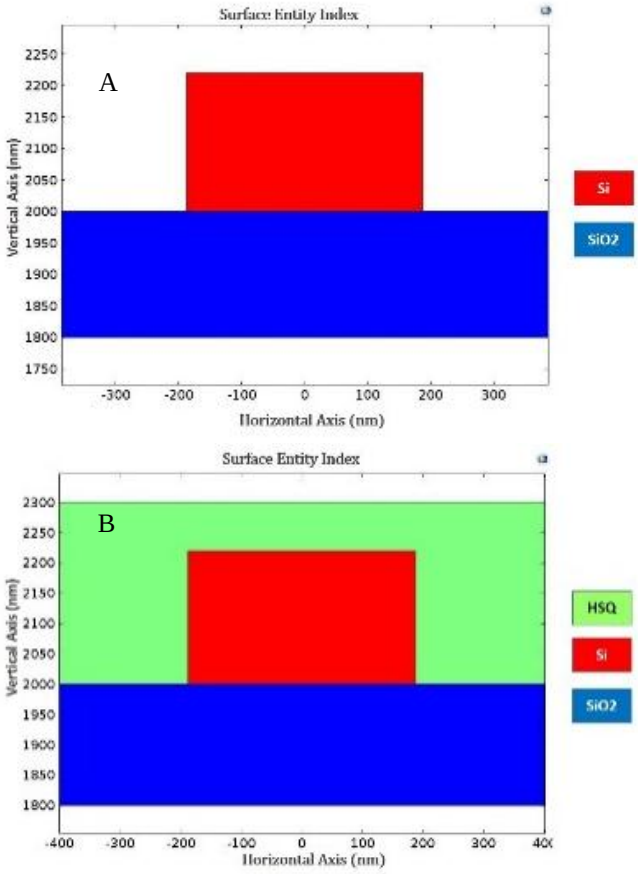

Figure 10. Steps used to design a waveguide GBOM using 2D COMSOL environment a- First step b- Second step

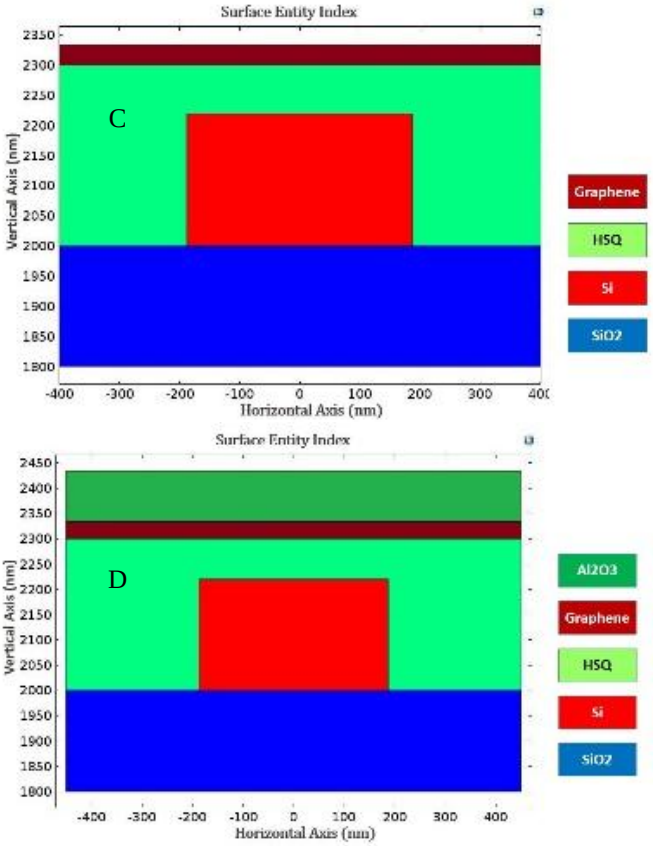

Figure 10. Steps used to design a waveguide GBOM using 2D COMSOL environment c- Third Step d- Fourth step.

IV. Simulation Results

Simulation is presented for the mode analysis of the designed modulators using COMSOL and LUMERICAL softwares. The graphene material is not found in the material library of these software packages. Therefore, one should make a model for graphene to support the design and the simulation process using the optoelectronic propertied deduced earlier.

A. Mode Analysis for Square Waveguide Modulators Using COMSOL

The mode analysis is done using COMSOL with the fundamental mode transfer electric TE00 for multiple structure progressing schemes for waveguide (WG) modulator and Mach-Zehnder modulator. The consideration of electrode material, the gold (Au) and the nickel (Ni) are taken for comparison purposes. Results of the COMSOL design of the square waveguide modulators are illustrated in Fig. 11a-c.

By adding the HSQ layer to the structure, the effective mode index becomes as shown in Fig. 11b. The effective mode index is simulated for the final modulator design as shown in Fig. 11c.

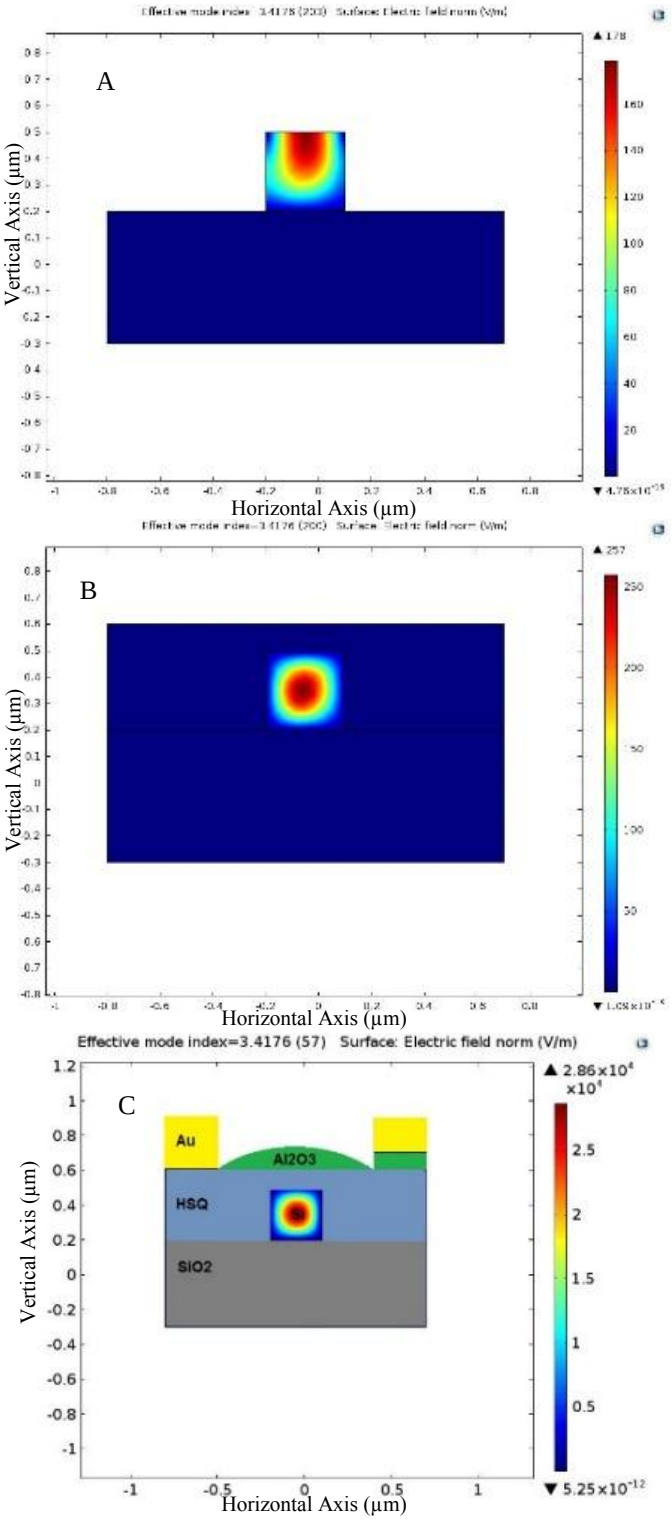

Figure 11. Effective mode index using a- Si waveguide and SiO_2 substrate b- Adding the HSQ layer c- Final modulator design.

The effective mode index is found to be 3.4176 for the three steps involved in the simulation process. The strong interaction of the guided mode is the advantage of the structure geometry design and material choice. For TE00, the surface

electric field varies in the steps of the design and this is a sign of convenient results. The surface electric field for the first step is at maximum of 178 V/m, for the second step is at maximum of 257 V/m, and for the final design is 2.68 X 10^6 V/m. Now considering the Mach-Zehnder modulator with a square waveguide shape. The three involved steps of the effective mode index simulation for TE00 mode, is shown in Fig. 12a-c. The effective mode index is simulated for the second step by adding the HSQ layer in the structure and the final step considering TE00 mode as shown in Fig. 12b-c, respectively.

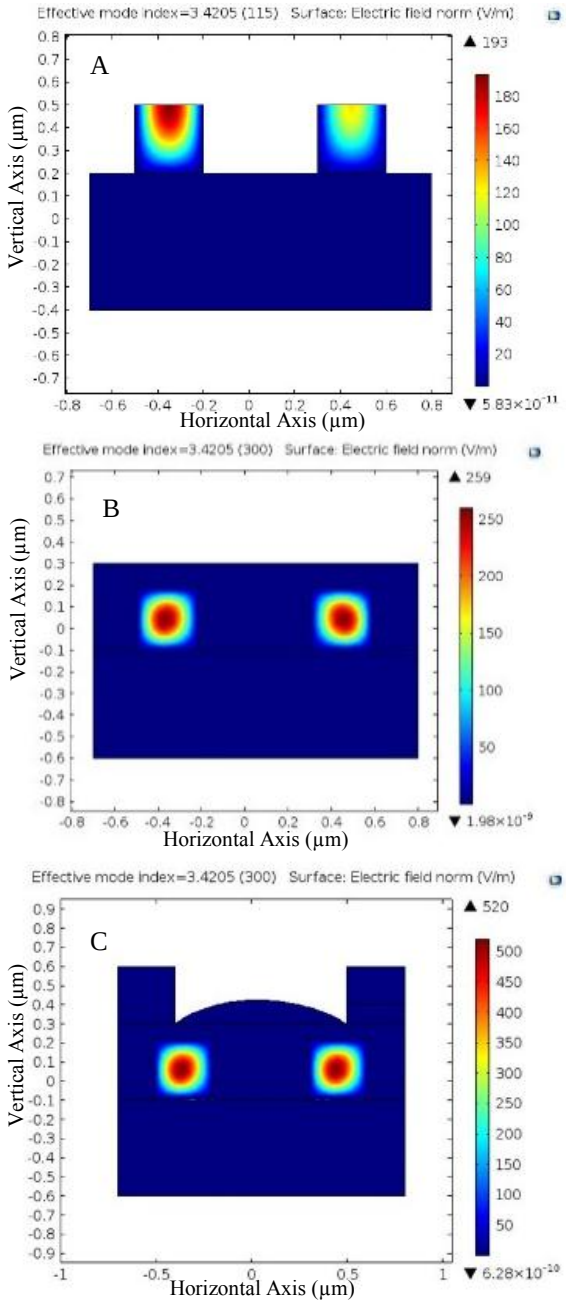

Figure 12. Mode analysis simulation result using MZM configuration. a- Si waveguide and SiO_2 substrate b- Adding the HSQ layer c- Final modulator design.

The mode analysis for the optical modulator is also done using the LUMERICAL. Fig. 13a shows the mode propagating inside the optical modulator. Fig. 13b shows the fundamental mode (TEM00) propagation inside the optical modulator.

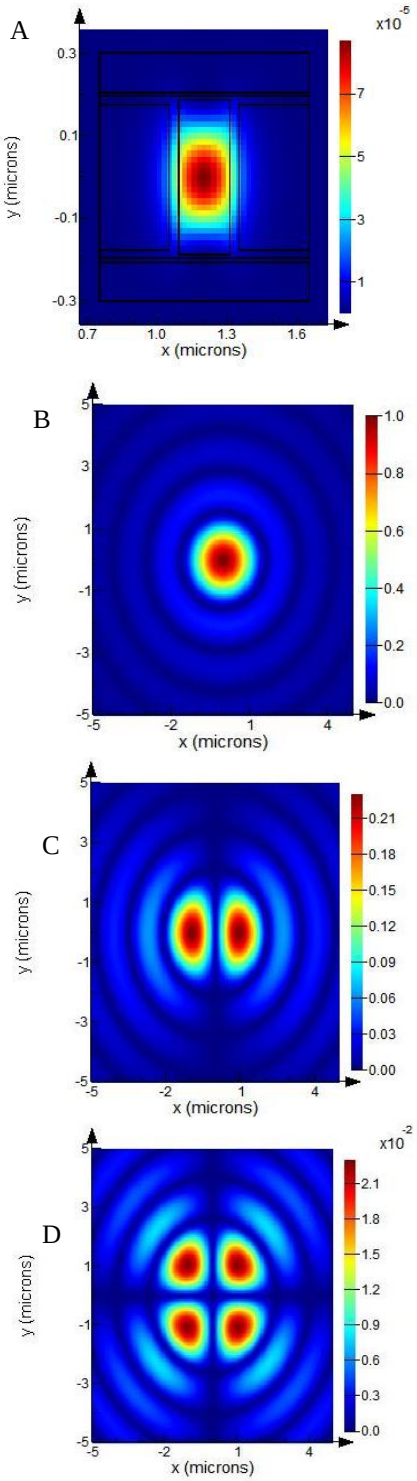

Figure 13. (a) The mode solution of the designed GBOM using LUMERICAL (b) TEM00 mode propagation (c, d) TEM10 and TEM11 mode propagation.

Fig. 13c shows the TEM10 and TEM11 mode propagation inside the optical modulator.

The mode analysis performed in both softwares shows that the effective mode index is 3.4176 and 3.4205 for the waveguide modulator and the MZM, respectively. Since the effective mode index does not have an imaginary part, this means no losses are found along the propagating modes. The phase constants (i.e. phase coefficients) of 1550 nm and 1310 nm operating wavelengths can be calculated from these results and they are listed in Table 2.

TABLE II. COMPARISON BETWEEN WGM AND MZM IN TERMS OF PROPAGATION CONSTANT AT 1550 NM AND 1310 NM.

	Waveguide Modulator	Mach-Zehnder Modulator
Effective mode index	3.4176	3.4205
Propagation constant at 1550 nm (rad/μm)	13.8538	13.8655
Propagation constant at 1310 nm (rad/μm)	16.3919	16.4058

The MZM modulator supports multimode operation and the number of modes that are calculated through the design simulation process is 257 mode. Fig. 14a and 14b show some of the modes that can propagate in the modulator with the near fundamental and higher-order modes, respectively.

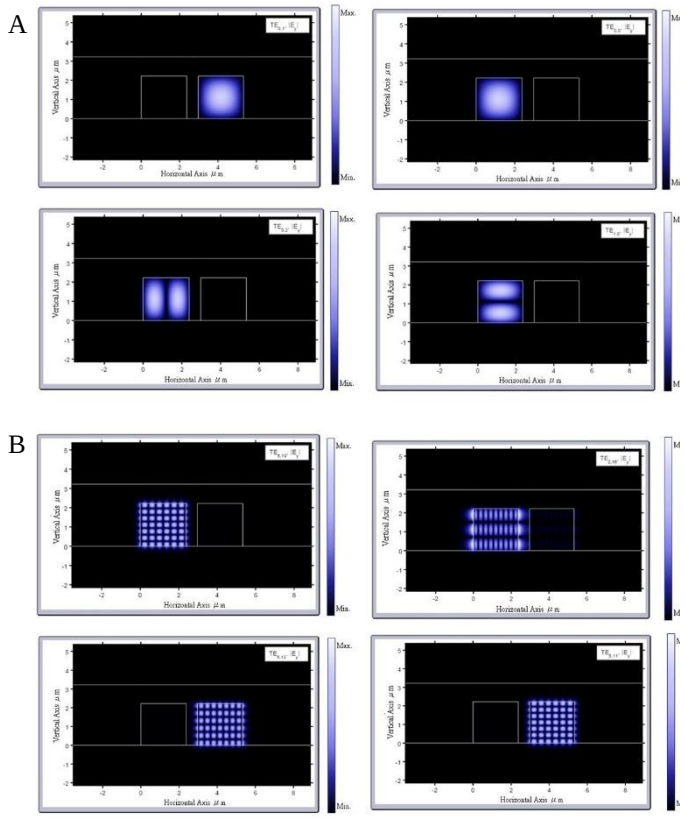

Figure 14. Mode analysis simulation result at the final step using MZM, a- Fundamental and near fundamental modes, b- Higher-order modes.

B. Mode Analysis for Rectangular Waveguide Modulators Using COMSOL

The mode analysis is done using COMSOL with the fundamental mode transfer electric TE00 from multiple structure progressing schemes for waveguide modulator and Mach-Zehnder modulator designed with rectangular cross-section silicon waveguide. Four steps are simulated for the WGM as illustrated in Fig. 15.

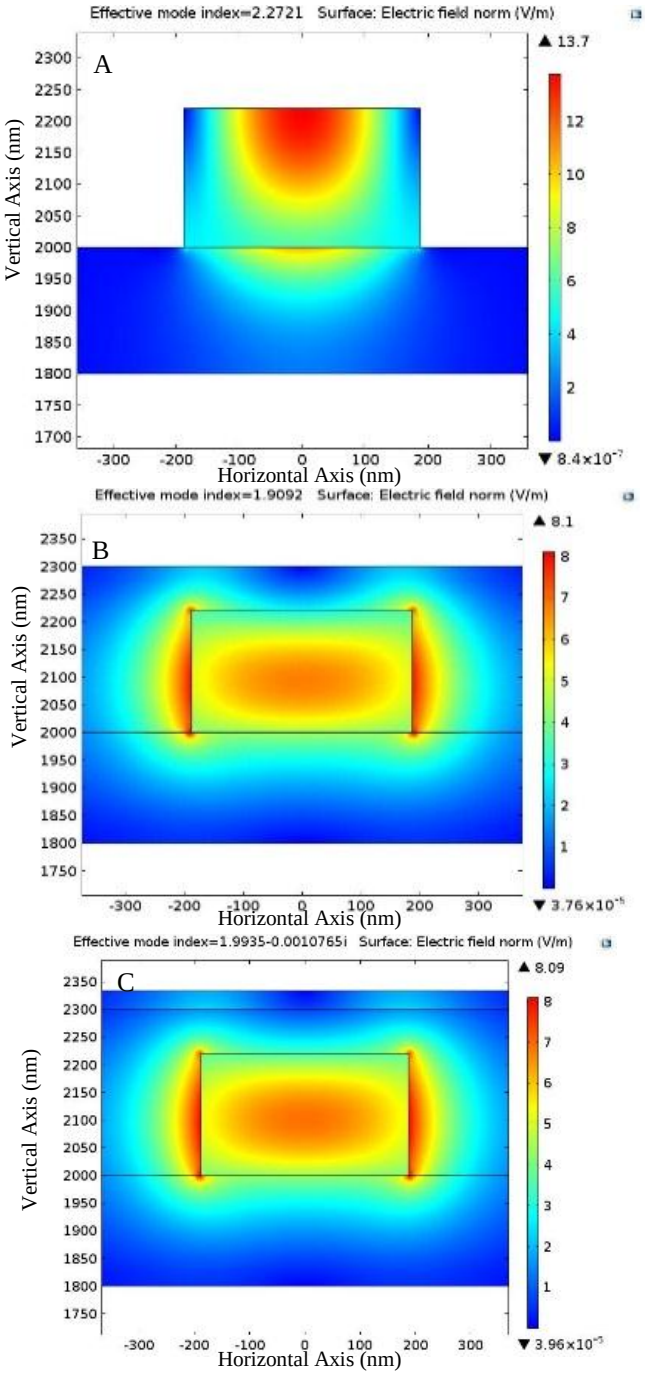

Figure 15. Mode analysis simulation result for 1550 nm WG modulator with rectangular shaped waveguide a- Si waveguide and SiO_2 substrate b- Adding the HSQ layer c- Adding graphene material

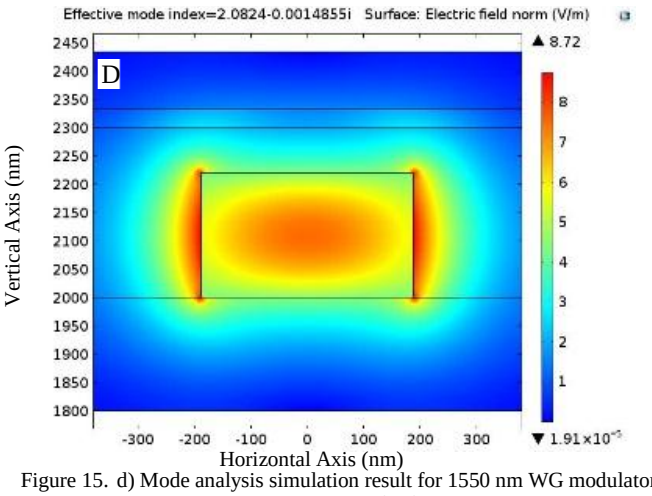

Figure 15. d) Mode analysis simulation result for 1550 nm WG modulator with rectangular shaped waveguide for final modulator design.

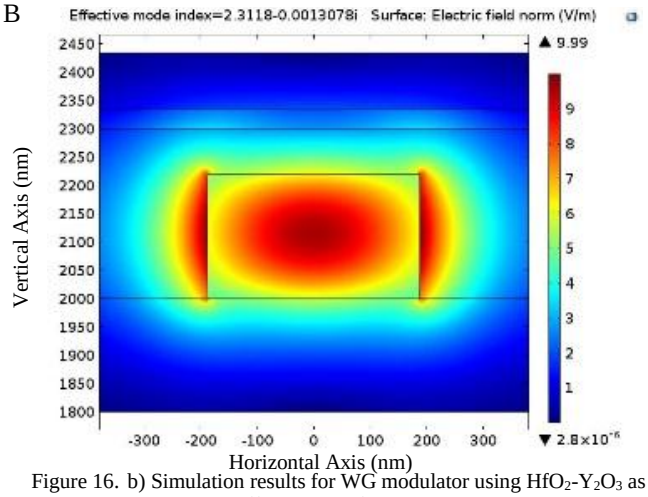

Figure 16. b) Simulation results for WG modulator using HfO_2-Y_2O_3 as a buffer material for 1310 nm.

i. Using SiO_2 as the base layer and add Si waveguide on top of it, (Fig. 15a).

ii. Adding HSQ as a buffer layer material (Fig. 15b).

iii. Adding graphene material on the top of the HSQ layer (Fig. 15c).

iv. Using Al2O3 material on the top of the structure (Fig. 15d).

The effective mode index for the WGM configuration design is found to be 2.2721, 1.9092, 1.9935 - 0.0010765i, 2.0824 -0.0014855i, for the first, second, third, and fourth step, respectively. The scale sensitivity is much higher when dealing with nm scale this is the result of the design accuracy. The surface electric field is at maximum of 13.7, 8.1, 8.09, 8.72 V/m for the first, second, third, and fourth step, respectively. The mode confinement is better enhanced by following the steps till the final design is obtained. This shows that the layout-geometry and material choice are quite accurate. Now considering the buffer layer material to be HfO_2-Y_2O_3.The simulation results are shown in Fig. 16a and 16b, for the wavelength of 1550 nm and 1310 nm, respectively.

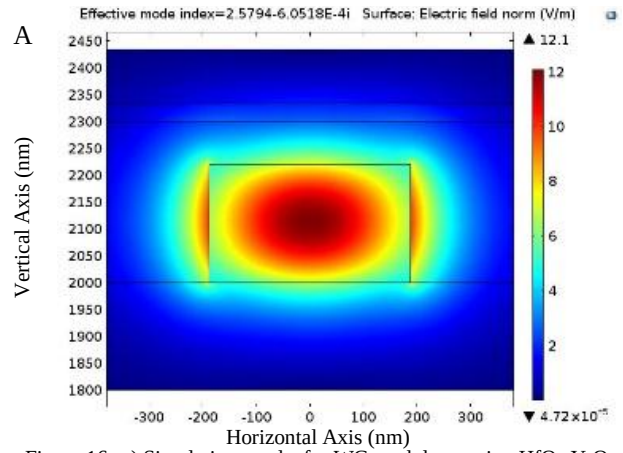

Figure 16. a) Simulation results for WG modulator using HfO_2-Y_2O_3 as a buffer material for 1550 nm.

The effective mode index (EMI) is calculated as 2.3118–0.0013078i, 2.5794 – 6.0518 X 10^{-4} for the wavelengths of 1550 nm and 1310 nm, respectively. The surface electric field is at maximum of 9.99 and 12.1 V/m for the wavelengths of 1550 nm and 1310 nm, respectively.

The Mach-Zehnder modulator is also designed and simulated for the case of using rectangular-shaped silicon waveguide. Four simulating steps are performed for the MZM modulator as follows

i. Using SiO_2 as the base layer and add Si waveguide on top of it, (Fig. 17a).

ii. Adding HSQ as a buffer layer material (Fig. 17b).

iii. Adding graphene material on the top of the HSQ layer (Fig. 17c).

iv. Using Al_2O_3 material on the top of the structure (Fig.17d).

The effective mode index for the MZM modulator configuration design is found to be 2.2708, 1.968, 2.0493 - 0.00075222i, 2.0697 – 0.0014014i, for the first, second, third, and fourth step, respectively. The scale sensitivity is much higher when dealing with nm scale this is the result of the design accuracy.

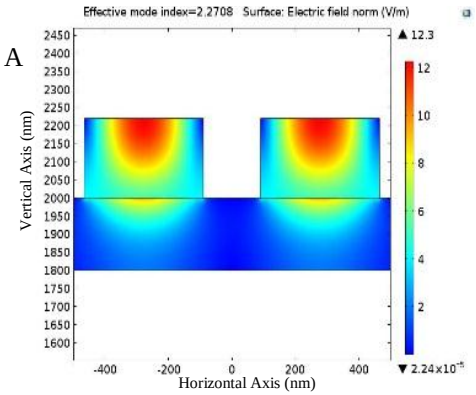

Figure 17. a) Mode analysis simulation result for 1550 nm MZM modulator of rectangular shaped waveguide using Si waveguide and SiO2 substrate.

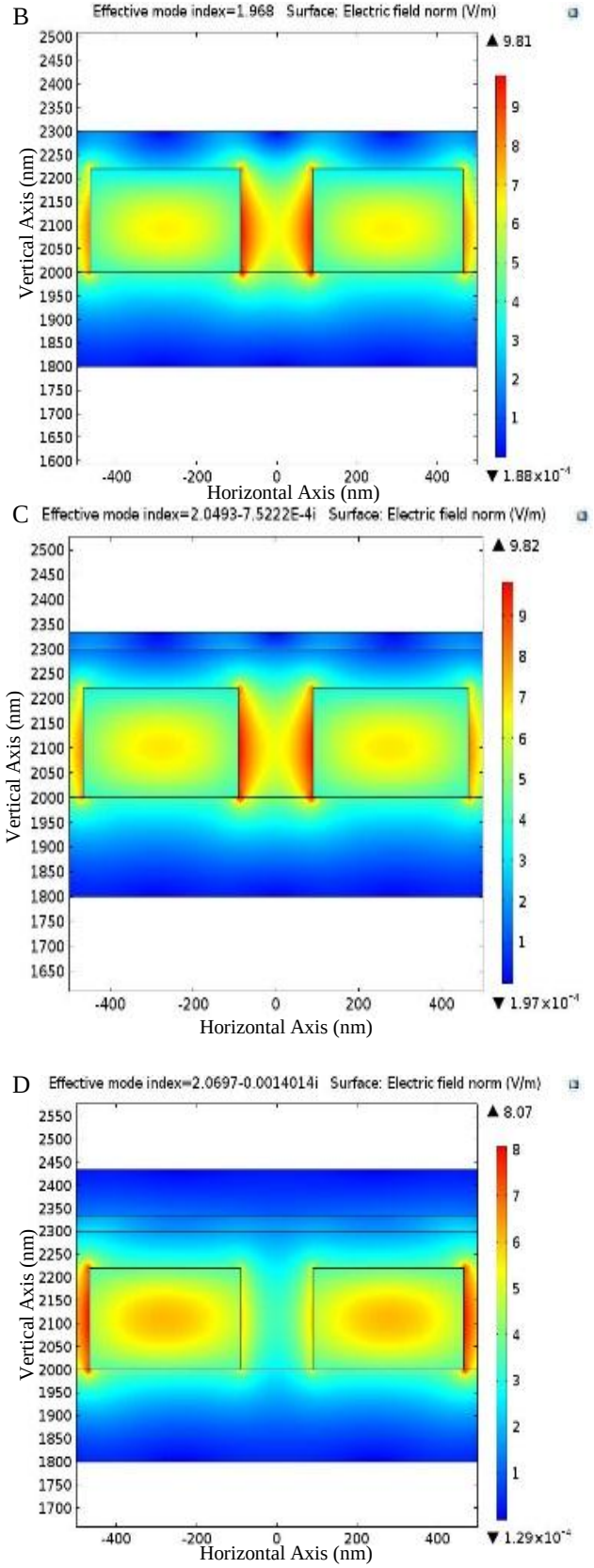

Figure 18. b,c,d) Mode analysis simulation result for 1550 nm MZM modulator of rectangular shaped waveguide b- Adding the HSQ layer c- Adding graphene material d- Final modulator design.

The surface electric field is at maximum of 12.3, 9.81, 9.82, 8.07 V/m for the first, second, third, and fourth step, respectively. The mode confinement is better enhanced by following the steps till the final design is obtained. This shows that the layout-geometry and material choice are quite accurate.

Now considering the buffer layer material to be HfO_2-Y_2O_3.The simulation results are shown in Fig. 18a and 18b for the wavelength of 1550 nm and 1310 nm, respectively.

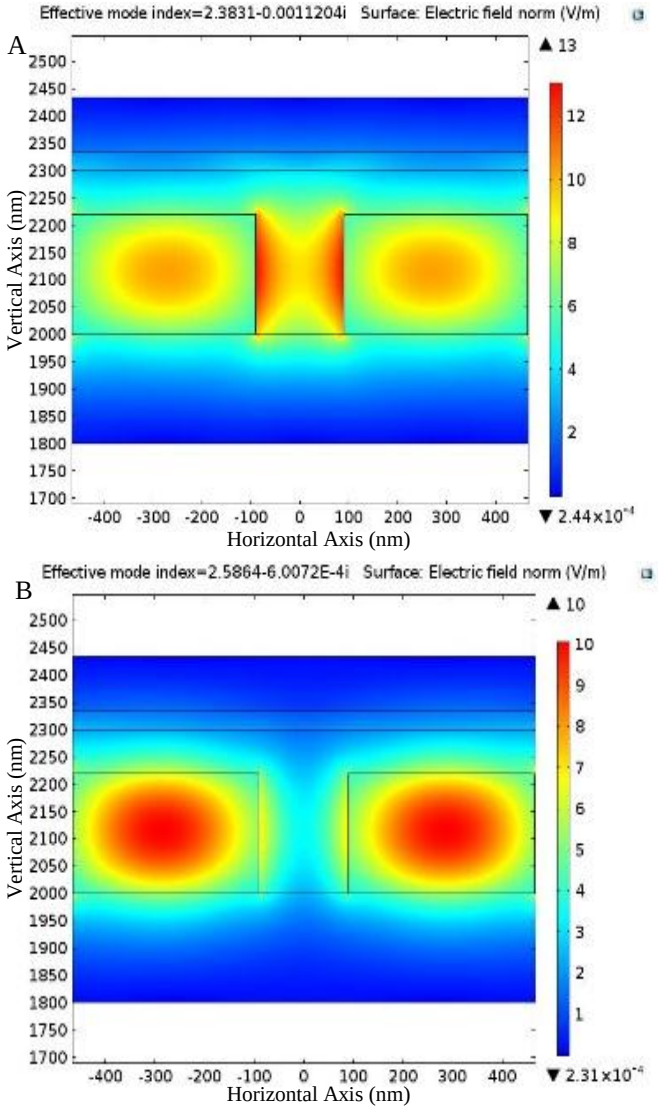

Figure 19. Simulation results for MZM modulator using HfO_2-Y_2O_3 as a buffer material for a- 1550 nm b- 1310 nm.

The effective mode index (EMI) is calculated as 2.3831 – 0.0011204i and 2.5864 – 6.0072 X 10^{-4} for the wavelengths of 1550 nm and 1310 nm, respectively. The surface electric field is at maximum of 13 and 10 V/m for the wavelengths of 1550 nm and 1310 nm, respectively.

The results that are obtained in the design in terms of time delay and maximum frequency (i.e. bandwidth) are provided

here for the four designed modulators. Two WG modulators having square and rectangular cross-section area and two related MZM modulators. Results are given for waveguide having arm lengths of 200 and 100 μm, and for 1550 and 1310 nm operating wavelengths, using HSQ as a buffer layer material, as shown in Table 3.

TABLE III. COMPARISON BETWEEN WG MODULATORS AND MZM MODULATORS IN TERMS OF TIME DELAY AND BANDWIDTH AT 200 AND 100 MM ARM LENGTH FOR WAVELENGTHS OF 1550 NM AND 1310 NM USING HSQ.

Designed Modulators		**Effective Mode Index (EMI)**	**Bandwidth (GHz)**		**Time Delay (ps)**	
Mod	***λ nm***		***100 μm***	***200 μm***	***100 μm***	***200 μm***
WG Sq.	1550	3.4176	219.4	109.7	1.12	2.25
	1310	3.4176	219.4	109.7	1.12	2.25
MZM Sq.	1550	3.4205	219.2	109.6	1.12	2.25
	1310	3.4205	219.2	109.6	1.12	2.25
WG Rect.	1550	2.0824–0.0014855i	360.1	180.1	0.68	1.37
	1310	2.4564-0.00052946i	305.3	152.6	0.81	1.62
MZM Rect.	1550	2.0697–0.0014014i	362.3	181.2	0.68	1.36
	1310	2.4708–0.00052327i	303.5	151.7	0.81	1.63

Table 4 shows the results when the four modulators are designed using HfO_2-Y_2O_3 as a buffer layer material.

TABLE IV. COMPARISON BETWEEN WG MODULATORS AND MZM MODULATORS IN TERMS OF TIME DELAY AND BANDWIDTH AT 200 AND 100 MM ARM LENGTH FOR WAVELENGTHS OF 1550 NM AND 1310 NM USING HfO_2-Y_2O_3.

Designed Modulators		**Effective Mode Index (EMI)**	**Bandwidth (GHz)**		**Time Delay (ps)**	
Mod	***λ nm***		***100 μm***	***200 μm***	***100 μm***	***200 μm***
WG Sq.	1550	3.48	215.5	107.8	1.15	2.3
	1310	3.48	215.5	107.8	1.15	2.3
MZM Sq.	1550	3.47	216.1	108.1	1.14	2.29
	1310	3.47	216.1	108.1	1.14	2.29
WG Rect.	1550	2.3118 – 0.0013078i	324.4	162.2	0.76	1.52
	1310	2.5794 – 0.0006051i	290.7	145.3	0.85	1.7
MZM Rect.	1550	2.3831 – 0.011204i	314.7	157.3	0.78	1.57
	1310	2.5864 – 0.0006007i	290	145	0.85	1.7

Investigating the results in this table reveals the following findings

i. Using rectangular cross section waveguide will enhance the bandwidth of the modulator by approximately 50 % and 35 % at 1550 nm and 1310 nm, respectively, compared with square cross section waveguide.

ii. Both WGM and MZM modulators have approximately the same bandwidth which scales inversely with the WG length.

Table 5 shows the results obtained for the three involved steps of the design of MZM modulator in terms of insertion loss, extinction ratio, and maximum and minimum transmission coefficients. T_{max} and T_{min}. The half-wave voltage is calculated for the four designed modulators with two arm lengths of 100 μm and 200 μm, respectively and the results are listed in Table 6.

TABLE V. RESULTS OF T_{MIN}, T_{MAX}, IL AND ER FOR THE THREE STEPS OF DESIGN.

Steps	**T_{min}**	**T_{max}**	**IL**	**ER**
HSQ + Al_2O_3	0.0199	0.1025	9.892	7.11
Graphene +Al_2O_3	0.4339	0.9950	0.021	3.6
Final Device	0.7051	0.9991	3.19×10^{-3}	1.5

TABLE VI. HALF-WAVE VOLTAGE CALCULATION RESULTS.

Arm lengths	**Mod 1**	**Mod 2**	**Mod 3**	**Mod 4**
	Half-Wave Voltage-Length Product $V_\pi L_\pi$ (V.cm)			
100 μm	0.8	0.4	0.2	0.01
200 μm	1.6	0.8	0.4	0.02

V. CONCLUSIONS

The paper has presented theoretical and simulation design steps and performance investigation for graphene-based optical modulators for 1550 nm and 1310 nm communication wavelengths. A theoretical model has been developed using surface conductivity to assess the graphene optoelectronic properties. The main conclusions drawn for this study are

i. The MZM is the prominent choice for the GBOM since it has a better confinement of the modes.

ii. Gold electrodes are more suitable than Nickel electrodes since they provide lower interaction noise and thus leave the modes with less interference.

iii. The minimum time delay is achieved using MZM modulator of a rectangular cross section and its 0.68 ps when the modulator is designed with 100 μm waveguide length which offers a bandwidth of 362.3 GHz.

iv. Using HfO_2-Y_2O_3 as a buffer layer material in the design of the modulators gives a higher EMI than HSQ material for the same design.

v. The half-wave voltage is reduced by using MZM configuration.

vi. Using rectangular cross section waveguide will enhance the bandwidth of the modulator by approximately 50 % and 35 % at 1550 nm and 1310 nm, respectively, compared with square cross section waveguide.

vii. Both WGM and MZM modulators have approximately the same bandwidth which scales inversely with the WG length.

REFERENCES

[1] D. Ponnamma, J. Kim and S. Thomas, "Graphene-Based Polymer Nanocomposites in Electronics", Springer International Publishing, Switzerland, PP. 197-198, (2015).

[2] W. Du, E. Li, and R. Hao, "Tunability Analysis of a Graphene-Embedded Ring Modulator", IEEE Photonics Technology Letters, Vol. 26, No. 20, PP. 2008-2011, Oct., (2014).

[3] S. Luo, Y. Wang, X. Tong and Z. Wang, "Graphene Based Optical Modulators", Nanoscale Research Letters, Vol. 10, No. 199, PP.1-11, Apr., (2015).

[4] W. Zhao, "Novel Metamaterials and Their Applications in Subwavelength Waveguides, Imaging and Modulation", Master Thesis, Rochester Institute of Technology, Rochester, New York, PP. 75-90, Feb., (2014).

[5] X. Chen and J. Yao, "A High Spectral Efficiency Coherent Microwave Photonic Link Employing Both Amplitude and Phase Modulation with Digital Phase Noise Cancellation", IEEE Journal of Lightwave Technology, Vol. 33, No. 14, PP. 3191-3197, Jul., (2015).

[6] D. Patel, A. Samani, V. Veerasubramanian, S. Ghosh, and D. Plant, "Silicon Photonic Segmented Modulator-Based Electro-Optic DAC for 100 Gb/s PAM-4 Generation", IEEE Photonics Technology Letters, Vol. 27, No. 23, PP. 2433-2436, Dec., (2015).

[7] K. Aoshima, K. Machida, D. Kato, T. Mishina, K. Wada, Y. Cai, H. Kinjo, K. Kuga, H. Kikuchi, T. Ishibashi, and N. Shimidzu, "A Magneto-Optical Spatial Light Modulator Driven by Spin Transfer Switching for 3D Holography Applications", Journal of Display Technology, Vol. 11, No. 2, PP. 129-135, Feb., (2015).

[8] A. Tiwari and M. Syvajarvi, "Graphene Materials Fundamentals and Emerging Applications", Wiley Publishing, PP. 3-20, (2015).

[9] V. Georgakilas, "Functionalization of Graphene", Wiley Publishing, PP.1-8, (2014).

[10] W. Zhu, I. Rukhlenko, and M. Premaratne, "Graphene Metamaterial for Optical Reflection Modulation", Applied Physics Letters, Vol. 102, Article No. 24194, PP. 1-4, Aug., (2013).

[11] Y. Gao, X. Gan, R. Shiue, K. Mak, X. Yao, L. Li, A. Szep, D. Walker, J. Hone, T. Heinz, and D. Englund, " Electro-optical Modulation in Graphene Integrated Photonic Crystal Nanocavities", IEEE Conference on Lasers and Electro-Optics (CLEO), Vol. 22, No. 21, PP. 1-2, Jul., (2013).

[12] F. Zhou, R. Hao, X. Jin, X. Zhang, and E. Li, "A Graphene-Enhanced Fiber-Optic Phase Modulator with Large Linear Dynamic Range", IEEE Photonics Technology Letters, Vol. 26, No. 18, PP. 1867-1870, Sep., (2014).

[13] S. Ye, Z. Wang, L. Tang, Y. Zhang, R. Lu, and Y. Liu, "Electro-Absorption Optical Modulator Using Dual-Graphene-on-Graphene Configuration", Optics Express, Vol. 22, No. 21, PP. 26137-26180, Oct., (2014).

[14] W. Du, E. Li, and R. Hao, "Tunability Analysis of a Graphene-Embedded Ring Modulator", IEEE Photonics Technology Letters, Vol. 26, No. 20, PP. 2008-2011, Oct., (2014).

[15] U. Ralevic, G. Isic, B. Vasic and R. Gajic, "Modulating Light With Graphene Embedded Into an Optical Waveguide", Applied Physics Letters, Vol. 47, Article No. 335101, PP. 1-9, Jul., (2014).

[16] M. Midrio, V. Sorianello, and M. Romagnoli, "Design Optimization of Single and Double Layer Graphene Phase Modulators in SOI", Optics Express, Vol. 23, No. 5, PP. 6478-6490, Mar., (2015).

[17] T. Pan, C. Qiu, J. Wu, X. Jiang, B. Liu, Y. Yang, H. Zhou, R. Soref, and Y. Su, "Analysis of an Electro-Optic Modulator Based on a Graphene-Silicon Hybrid 1D Photonic Crystal Nanobeam Cavity", Optics Express, Vol. 23, No. 18, PP. 23357- 23364, Sep., (2015).

[18] M. Midrio, P. Galli, M. Romagnoli, L. Kimerling, and J. Michel, "Graphene-Based Optical Phase Modulation of Waveguide Transverse Electric Modes", Journal of Photonics Research, Vol. 2, No. 3, PP. A34-A40, Jun., (2014).

[19] R. Hao and J. Jin, "Graphene Embedded Modulator with Extremely Small Footprint and High Modulation Efficiency", Journal of Photonics, Vol. 2014, Article No. 309350, PP. 1-6, May, (2014).

[20] Y. Hu, M. Pantouvaki, S. Brems, I. Asselberghs, C. Huyghebaert, M. Geisler, C. Alessandri, R. Baets, P. Absil, D. Thourhout and J. Campenhout, "Broadband 10Gb/s Graphene Electro-Absorption Modulator on Silicon for Chip-Level Optical Interconnects", IEEE International Electron Devices Meeting (IEDM), Vol.14, Article No. 128, PP. 1-4, (2014).

[21] M. Mohsin, D. Schall, M. Otto, A. Noculak, D. Neumaier, and H. Kurz, "Graphene Based Low Insertion Loss Electro Absorption Modulator on SOI Waveguide", Optics Express, Vol. 22, No. 12, PP. 15292- 15297, Jun., (2014).

[22] M. Mohsin, D. Neumaier, D. Schall, M. Otto, C. Matheisen, A. Giesecke, A. Sagade and H. Kurz, "Experimental Verification of Electro-Refractive Phase Modulation in Graphene", Nature Scientific Reports, PP. 1-7, Jun., (2015).

[23] C. Phare, Y. Lee, J. Cardenas and M. Lipson, "Graphene Electro-Optic Modulator with 30 GHz Bandwidth", Nature Photonics, Vol. 9, PP. 511-514, Aug., (2015).

[24] A. Geim and K. Novoselov, "The Rise of Graphene", Manchester Centre for Mesoscience and Nanotechnology, University of Manchester, Oxford Road, United Kingdom, PP. 1-14, (2004).

[25] S. Koester and M. Li, "Waveguide-Coupled Graphene Optoelectronics", IEEE Journal of Selected Topics in Quantum Electronics, Vol. 20, No.1, PP. 1-3, Jan., (2014).

[26] J. Capmany, D. Domenech and P. Munoz, "Graphene Integrated Microwave Photonics", IEEE Journal of Lightwave Technology, Vol. 32, No. 20, PP. 3785-3788, Oct., (2014).

[27] J. Capmany, D. Domenech and P. Muñoz, "Silicon Graphene Reconfigurable CROWS and SCISSORS", IEEE Journal of Photonics, Vol. 7, No. 2, PP. 1-4, Apr. (2015).

[28] C. Xu, Y. Jin, L. Yang, J. Yang, and X. Jiang, "Characteristics of Electro-Refractive Modulating Based on Graphene-Oxide-Silicon Waveguide", Optics Express, Vol. 20, No. 20, PP. 22400-22404, Sep. (2012).

[29] W. Zhu, I. Rukhlenko, and M. Premaratne, "Graphene Metamaterial for Optical Reflection Modulation", Applied Physics Letters, No. 102, Article No. 241914, PP. 1-3, Jun. (2013).

[30] C. Rao and A. Sood, "Graphene: Synthesis, Properties, and Phenomena", Wiley-VCH Verlag and Co. KGaA, PP. 141,252-255, (2013).

[31] W. Fan, Chao Zhang, W. Tjiu, and T. Liua, "Fabrication of Electrically Conductive Graphene/Polystyrene Composites via a Combination of Latex and Layer-by-Layer Assembly Approaches", Journal of Materials Research, Vol. 28, No. 4, PP. 611-619, Feb., (2012).

[32] M. Lemme, "Potential Applications for Graphene Devices in Nano-electronics", KTH Royal Institute of Technology, School of Information and Communication Technology, PP. 4-7, (2012).

[33] L. Falkovsky, "Optical Properties of Graphene", Journal of Physics, the International Conference on Theoretical Physics, No. 129, PP. 1-7, (2008).

[34] J. Horng, C. Chen, B. Geng, C. Girit, Y. Zhang, Z. Hao, H. Bechtel, M. Martin, A. Zettl, M. Crommie, Y. Shen, and F. Wang, "Intraband Optical Transitions in Graphene", Conference on Lasers and Electro-Optics (CLEO), PP. 1-2, (2011).

[35] N. Shen, P. Tassin, T. Koschny, and C. Soukoulis, "Comparison of Gold- and Graphene-Based Resonant Nanostructures for Terahertz

Metamaterials and an Ultrathin Graphene-Based Modulator", Physical Review, Article No. 115437, PP. 1-8, (2014).

[36] A. Zak, "Bow-Tie Antenna-Coupled Graphene FETs for Direct Detection at 0.6THz", Master Thesis in Nanoscience and Nanotechnology, Chalmers University of Technology, Gothenburg, Sweden, PP. 3-6, (2014).

[37] S. Shafraniuk, "Graphene: Fundamentals, Devices, and Applications", Taylor and Francis, PP. 5-9, (2015).

[38] J. Gosciniak, D. Tan and B. Corbett, "Enhanced Performance of Graphene-Based Electro-Absorption Waveguide Modulators by Engineered Optical Modes", Applied Physics, Vol. 48, Article No. 235101, PP. 4, (2015).

Raad Sami Fyath was born in Maysan, Iraq, in 1954. He received the B.Sc. degree in Electrical Engineering from the University of Basrah, Iraq, in 1976, the M.Sc. degree in Electronics and Communications Engineering from the University of Baghdad, Iraq, in 1987, and the PhD degree in Electronics Engineering from University of Wales-Bangor, UK, in 1990. Currently, he is a professor of electronics and communications engineering at the College of Engineering, Alnahrain University, Baghdad, Iraq. His research interests include Optical and wireless communications, Optoelectronics, and Nanophotonics. He published more than 100 papers in different scientific journals and conference proceedings.

Taif Aied Faisal was born in Baghdad, Iraq, in 1992. He received the B.Sc. degree in Laser and Optoelectronics Engineering from Al-Nahrain University, Baghdad, Iraq, in 2013, and currently working toward M.Sc. degree in Laser and Optoelectronics Engineering from Al-Nahrain University. He had an experience in communication and telecommunication systems gained from his work with Earthlink Company, Iraq, in 2014.